Density Field Dynamics: Scalar Refractive Gravity, Quantum Resolution, and Dual-Sector Electrodynamics

Gary Alcock
Los Angeles, CA, USA
(Dated: October 1, 2025)

We develop Density Field Dynamics (DFD), a scalar-field framework in which a single refractive index field $\psi(\mathbf{x},t)$ replaces curved spacetime. Light propagates with optical index $n = e^{\psi}$, matter accelerates as $\mathbf{a} = (c^2/2)\nabla\psi$, and ψ obeys a nonlinear Poisson equation. This reproduces all classical weak-field tests of General Relativity (deflection, redshift, Shapiro, perihelion), matches PPN at $\mathcal{O}(1/c^2)$, and explains galactic dynamics without dark matter via the crossover function $\mu(|\nabla\psi|/a_\star)$.

DFD offers a clean resolution of the Penrose measurement paradox: superpositions always source a single ψ field, eliminating the "two geometries" problem, while quantum evolution in this background remains strictly unitary. We contrast DFD with Diósi–Penrose (DP) objective reduction, and state a quantitative prediction: *null* deviations from unitary quantum mechanics in regimes targeted at DP collapse times.

Finally, we show that in the dual-sector extension, Maxwell electrodynamics is consistently embedded in a ψ-dependent vacuum. A controlled ϵ/μ split preserves the optical metric speed $v_{\rm ph} = c/n$, while ψ-gradients and time-variation yield small, falsifiable corrections. Faraday induction remains $\nabla \times \mathbf{E} = -\partial_t \mathbf{B}$ (a Bianchi identity); the dual sector explains the *sectoral response* (electric vs. magnetic) through the split, not by altering the identity. The same bracket $[B^2/\mu - \epsilon E^2]$ governs ψ sourcing, energy exchange, and body force, with concrete predictions in cavity and clock experiments. We parameterize the split as $g(\psi) = \kappa\psi$ and show how κ is constrained and *measured* by sector-resolved LPI slopes.

I. CORE POSTULATES OF DFD

1. Light propagation:

$$n(\mathbf{x}) = e^{\psi(\mathbf{x})}, \qquad c_1(\mathbf{x}) = \frac{c}{n} = c\,e^{-\psi}. \tag{1}$$

2. Matter dynamics:

$$\mathbf{a} = \frac{c^2}{2}\nabla\psi \equiv -\nabla\Phi, \quad \Phi \equiv -\tfrac{c^2}{2}\psi. \tag{2}$$

3. Field equation (nonlinear Poisson form):

$$\nabla\cdot\left[\mu(|\nabla\psi|/a_\star)\nabla\psi\right] = -\frac{8\pi G}{c^2}(\rho - \bar\rho). \tag{3}$$

Normalization by $-8\pi G/c^2$ fixes GR's optical tests (deflection, redshift, Shapiro).

II. CLASSICAL TESTS AND PPN

A. Newtonian limit

For point mass M with $\mu \to 1$:

$$\psi(r) = \frac{2GM}{c^2 r}, \quad \mathbf{a} = -\frac{GM}{r^2}\hat{\mathbf{r}}. \tag{4}$$

B. Light deflection, redshift, delay

With $n \simeq 1 + \psi$:

$$\alpha = \frac{4GM}{c^2 b}, \tag{5}$$
$$\frac{\Delta\nu}{\nu} = -\frac{\Delta\Phi}{c^2}, \tag{6}$$
$$\Delta t = \frac{4GM}{c^3}\ \text{(two-way)}. \tag{7}$$

C. PPN check

Expanding DFD to $\mathcal{O}(1/c^2)$ reproduces $\gamma = \beta = 1$, all others 0 [6].

III. PENROSE PARADOX, SCHRÖDINGER DYNAMICS, AND DP COMPARISON

A. One ψ for superpositions: existence and uniqueness

Penrose argued that a mass superposition implies a superposition of geometries, in conflict with the single Hilbert space of quantum mechanics [9–11]. In DFD, mass density enters the sourcing equation linearly, so for a superposition state $|\Psi\rangle = \sum_i c_i |M_i\rangle$ the effective density is

$$\rho_{\text{eff}}(\mathbf{x}) = \langle\Psi|\hat{\rho}(\mathbf{x})|\Psi\rangle = \sum_i |c_i|^2 \rho_i(\mathbf{x}). \tag{8}$$

The field equation is elliptic with monotone μ, so standard theorems guarantee existence and uniqueness of a *single* ψ solution for given ρ_{eff} (no branch geometries).

B. Justifying the Schrödinger operator

We now justify the modified kinetic operator

$$i\hbar\,\partial_t\Psi = -\frac{\hbar^2}{2m}\,\nabla\cdot\left(e^{-\psi}\nabla\Psi\right) + m\Phi\,\Psi, \qquad \Phi = -\tfrac{c^2}{2}\psi, \tag{9}$$

by three mutually consistent routes:

(i) Hamiltonian and classical limit. Take the single-particle Hamiltonian

$$H(\mathbf{x},\mathbf{p}) = \frac{e^{-\psi(\mathbf{x})}}{2m}\,p^2 + m\Phi(\mathbf{x}). \tag{10}$$

Hamilton's equations give $\dot{\mathbf{x}} = e^{-\psi}\mathbf{p}/m$ and

$$\dot{\mathbf{p}} = -\nabla H = -\frac{p^2}{2m}\,\nabla(e^{-\psi}) - m\nabla\Phi = +\frac{p^2}{2m}\,e^{-\psi}\nabla\psi - m\nabla\Phi. \tag{11}$$

In the non-relativistic regime $p^2/2m \ll mc^2$, the force is dominated by $-m\nabla\Phi = (mc^2/2)\nabla\psi$, yielding $\mathbf{a} = (c^2/2)\nabla\psi$ as required by DFD. Quantizing H with a symmetric-ordering prescription $p^2 \mapsto -\hbar^2\nabla\cdot(\cdot)\nabla$ yields Eq. (9).

(ii) WKB/Hamilton–Jacobi. Insert $\Psi = A\,e^{iS/\hbar}$ into Eq. (9); to leading order in $\hbar$ one obtains the Hamilton–Jacobi equation

$$\partial_t S + \frac{e^{-\psi}}{2m}|\nabla S|^2 + m\Phi = 0, \tag{12}$$

with $\mathbf{p} = \nabla S$; this is exactly the classical Hamiltonian (10). The next order gives the continuity equation with probability current

$$\mathbf{j} = \frac{\hbar}{2mi}\left(\Psi^* e^{-\psi}\nabla\Psi - \Psi\,e^{-\psi}\nabla\Psi^*\right), \tag{13}$$

which is conserved, confirming self-adjointness.

(iii) Covariant wave in optical metric. The optical metric viewpoint sets $ds^2 = -c^2 e^{-2\psi} dt^2 + d\mathbf{x}^2$ for phase propagation (eikonal). The minimally coupled scalar wave operator $\Box_{\rm opt}\Psi = 0$ reduces in the nonrelativistic limit to Eq. (9) with $v_{\rm ph} = c/n$ (details omitted for brevity; see also matter-wave derivations in [7, 8]).

C. DP collapse vs. DFD prediction (quantitative)

DP proposes gravity-induced objective reduction with collapse time $\tau_{\rm DP} \sim \hbar/\Delta E_G$ where ΔE_G is the gravitational self-energy of the *difference* density between branches [11–13]. For a simple toy estimate of two identical lumps of mass m separated by d,

$$\Delta E_G \sim \frac{Gm^2}{d}, \qquad \tau_{\rm DP} \sim \frac{\hbar d}{Gm^2}. \tag{14}$$

Examples:

- *Large molecules (tested):* $m \sim 10^4$ amu $\simeq 1.7 \times 10^{-23}$ kg, $d \sim 100$ nm $\Rightarrow \tau_{\rm DP} \sim 5 \times 10^{15}$ s $\gg$ experimental timescales; both DP and DFD predict unitary evolution. (See [14–16].)
- *Mesoscopic spheres (future):* $m \sim 10^{-14}$ kg, $d \sim 1$ μm $\Rightarrow \Delta E_G \sim 6.7 \times 10^{-33}$ J, $\tau_{\rm DP} \sim 0.016$ s. Here DP predicts visible collapse; *DFD predicts null* (no intrinsic collapse). Cantilever and opto-mechanical bounds are approaching this region [17].

DFD prediction: For any platform claiming sensitivity to $\tau_{\rm DP} \lesssim 1$ s, expect *no* gravity-induced deviations from unitary QM (within stated uncertainties). The decisive DFD test remains the sector-resolved LPI slope (Sec. VIII), where GR predicts a strict null.

IV. SECTOR-RESOLVED LPI TEST

Compare cavity frequency ($f \sim c/n$) with atomic frequency across two altitudes Δh. Observable slope:

$$\frac{\Delta R}{R} = \xi^{(M,S)} \frac{\Delta \Phi}{c^2}, \tag{15}$$

with $\xi^{(M,S)} = \alpha_w - \alpha_L^{(M)} - \alpha_{at}^{(S)}$.
GR: $\xi = 0$. Base DFD: $\xi \simeq 1 \Rightarrow$ slope $\sim g\Delta h/c^2 \approx 1.1 \times 10^{-14}$ per 100 m.

V. MAXWELL ELECTRODYNAMICS IN A ψ-DEPENDENT VACUUM

We build on the classical foundations of Faraday's induction and field concept, Maxwell's field equations, Heaviside's vector reformulation, and standard modern expositions [1–5] by embedding Maxwell's equations in a ψ-dependent vacuum.

A. Constitutive split preserving $v_{\rm ph} = c/n$

$$\epsilon(\psi) = \epsilon_0\, n(\psi)\, e^{+\kappa\psi}, \qquad \mu(\psi) = \mu_0\, n(\psi)\, e^{-\kappa\psi}, \qquad n = e^{\psi}. \tag{16}$$

Here $\epsilon(\psi)$ and $\mu(\psi)$ vary oppositely such that their product tracks n^2/c^2, thereby preserving the optical-metric phase speed $v_{\rm ph} = c/n$.

$$\epsilon(\psi)\mu(\psi) = \epsilon_0\mu_0\, n^2 \quad \Rightarrow \quad v_{\rm ph} = \frac{1}{\sqrt{\epsilon(\psi)\mu(\psi)}} = \frac{c}{n}. \tag{17}$$

B. Variational equations

Action

$$\mathcal{L} = \mathcal{L}_\psi - \tfrac{1}{2}\epsilon(\psi)\mathbf{E}^2 + \tfrac{1}{2\mu(\psi)}\mathbf{B}^2 + \mathbf{J}\cdot\mathbf{A} - \rho\phi. \tag{18}$$

Varying ϕ and $\mathbf{A}$ yields Maxwell in a ψ-dependent medium:

$$\nabla\cdot(\epsilon\mathbf{E}) = \rho, \tag{19}$$
$$\nabla\times\mathbf{H} = \mathbf{J} + \partial_t\mathbf{D}, \tag{20}$$
$$\nabla\times\mathbf{E} = -\partial_t\mathbf{B}, \qquad \nabla\cdot\mathbf{B} = 0, \tag{21}$$

with $\mathbf{D} = \epsilon\mathbf{E}$, $\mathbf{H} = \mathbf{B}/\mu$.

C. Corrections from $\nabla\psi$ and $\dot\psi$

Ampère's law acquires

$$\nabla\times\mathbf{B} = \mu\mathbf{J} + \frac{1}{c^2}\partial_t\mathbf{E} + \frac{\kappa}{c^2}\dot\psi\,\mathbf{E} - \kappa(\nabla\psi\times\mathbf{B}). \tag{22}$$

Corrections vanish for uniform ψ; appear in gradients/time variation. Faraday and $\nabla\cdot\mathbf{B} = 0$ remain identities.

D. Energy, momentum, and sourcing

EM energy density and flux:

$$u = \tfrac{1}{2}(\epsilon\mathbf{E}^2 + \mathbf{B}^2/\mu), \qquad \mathbf{S} = \mathbf{E}\times\mathbf{H}. \tag{23}$$

Poynting theorem:

$$\partial_t u + \nabla\cdot\mathbf{S} = -\mathbf{J}\cdot\mathbf{E} - \tfrac{\kappa}{2}\,\dot\psi\left(\epsilon\mathbf{E}^2 - \frac{\mathbf{B}^2}{\mu}\right). \tag{24}$$

Body force:

$$\mathbf{f}_\psi = -\tfrac{\kappa}{2}\left(\frac{\mathbf{B}^2}{\mu} - \epsilon\mathbf{E}^2\right)\nabla\psi. \tag{25}$$

ψ sourcing:

$$\frac{\delta\mathcal{L}_\psi}{\delta\psi} = \mathcal{S}_{\rm mass} + \tfrac{\kappa}{2}\left(\frac{\mathbf{B}^2}{\mu} - \epsilon\mathbf{E}^2\right). \tag{26}$$

Thus the unified bracket governs energy exchange, momentum transfer, and scalar sourcing.

VI. STANDING-WAVE ENERGY EQUALITY (AND WHERE IMBALANCE ENTERS)

For a lossless, steady-state standing wave in a linear medium, the cycle-averaged *integrated* electric and magnetic energies are equal:

$$\int_V \overline{\epsilon E^2}\,dV \;=\; \int_V \overline{B^2/\mu}\,dV, \tag{27}$$

so $\int_V \overline{(B^2/\mu - \epsilon E^2)}\,dV = 0$. This follows from multiplying the wave equation by $\mathbf{E}$, integrating by parts, and using the steady-state condition; no appeal to the mechanical virial theorem is needed.

Nonzero *local* bracket arises at $\mathcal{O}(\theta^2)$ due to longitudinal fields in paraxial Gaussian modes (Sec. VII); it matters (i) when weighted by $\nabla\psi$ in the body-force channel, and (ii) for polarization/mode mixing tests (TE vs. TM). It does *not* dominate the LPI slope, which is set by sector coefficients.

VII. CAVITY MODE EXAMPLE

For a Fabry–Pérot resonator in TEM_{00}:

$$E_x = E_0 \cos(kz)\, e^{-(x^2+y^2)/w_0^2}, \tag{28}$$

$$B_y = \tfrac{E_0}{c} \sin(kz)\, e^{-(x^2+y^2)/w_0^2}. \tag{29}$$

By Eq. (27), $\int (B^2/\mu - \epsilon E^2) dV = 0$ (time-averaged, integrated).

Paraxial longitudinal components generate a *local* imbalance at $\mathcal{O}(\theta^2)$:

$$\overline{\epsilon E^2} - \overline{B^2/\mu} \sim \theta^2\, \epsilon |E_0|^2, \qquad \theta = \frac{\lambda}{\pi w_0}. \tag{30}$$

For $\lambda = 1064$ nm, $w_0 = 300\,\mu$m, $\theta^2 \simeq 1.3 \times 10^{-6}$. Implications: (i) the global LPI slope is dominated by sector coefficients (next section), (ii) TE/TM swaps and orientation provide clean internal nulls/cross-checks. *These parameter choices and cavity/clock operating regimes are representative of state-of-the-art platforms used in ultra-stable resonators and optical clocks [27–29].*

VIII. LPI PREDICTION WITH κ (QUANTITATIVE)

The slope is

$$\xi^{(M,S)}(\kappa) = 1 - \alpha_L^{(M)} - \alpha_{\rm at}^{(S)}(\kappa), \qquad \alpha_{\rm at}^{(S)}(\kappa) = K_\epsilon^{(S)}\, \kappa + \mathcal{O}(\kappa^2), \tag{31}$$

where $K_\epsilon^{(S)}$ is the (dimensionless) atomic EM-energy sensitivity.

Order-of-magnitude for $K_\epsilon^{(S)}$. Atomic optical transition energies scale with the effective Rydberg $R_\infty \propto 1/\epsilon^2$ (in SI), modulo relativistic and many-body corrections; thus a crude estimate gives

$$\left.\frac{\delta E}{E}\right|_{\rm gross} \simeq -2\, \frac{\delta\epsilon}{\epsilon} \quad \Rightarrow \quad K_\epsilon^{(S)} \sim \mathcal{O}(1\text{–}3), \tag{32}$$

with species/line dependence (fine/hyperfine and configuration mixing modify the coefficient). For Sr and Yb clock transitions, $K_\epsilon^{(S)}$ is plausibly order unity; the sector-resolved 4→3 GLS disentangles $\delta_{\rm at} \propto K_\epsilon^{(S)}\kappa$ from material (δ_L) and total ($\delta_{\rm tot}$) combinations.

Numbers. Keep the base prediction $|\Delta R/R| \approx g\Delta h/c^2 \simeq 1.1 \times 10^{-14}$ per 100 m. The dual-sector introduces an order-unity modulation of ξ if $K_\epsilon^{(S)}\kappa \sim 1$. Polarization (TE/TM) and dual-λ checks separate this from dispersion/thermals.

IX. EXISTING BOUNDS ON κ AND RELATED SEARCHES

PPN and optical tests. DFD matches GR at 1PN [6]; choosing the nondispersive band with $v_{\rm ph} = c/n$ preserved ensures solar-system optics are unaltered.

Why metrology has not already seen it. Most precision tests are *two-way* or single-sector: they cancel the sectoral response. The LPI ratio is a *sector comparison* under $\Delta\Phi/c^2$ change with internal nulls (swap/flip/dual-λ).

Cavity stability (accidental bound). Absence of 2ω parametric instabilities in extreme-Q resonators constrains unintended EM$\leftrightarrow$ ψ pumping. This provides headroom consistent with $|\kappa|$ below order unity; a dedicated LPI measurement is still required to bound/measure κ.

Altitude/diurnal constraints. A pure cavity-to-cavity comparison at different altitudes largely *tracks n* (common-mode) and does not isolate κ; the dual-sector signature appears most cleanly in *cavity vs. atom* ratios with identical geopotential steps. Diurnal solar tides ($\Delta\Phi/c^2 \sim 10^{-10}$) imply fractional modulations $\sim \xi\, 10^{-10}$; current clock comparisons place strong LPI bounds on generic $\alpha(\Phi)$-type couplings [18–20], but those do not directly exclude a *sectoral* κ that cancels in single-sector measurements. The proposed sector-resolved LPI explicitly avoids such cancellations.

LLI / Michelson–Morley modern tests. Modern rotating-cavity experiments bound anisotropies in the speed of light at $\sim 10^{-17}$–10^{-18} [23, 24]. Our construction preserves two-way c and embeds Maxwell consistently, so these tests are satisfied by design.

Equivalence principle & varying α. MICROSCOPE bounds differential acceleration at $\eta \lesssim 10^{-15}$ (final analysis) [25, 26]; DFD's matter acceleration is universal at given ψ so EP is respected. Constraints on $\dot{\alpha}/\alpha$ and $\alpha(\Phi)$ from clock comparisons exist at $\lesssim 10^{-16}$–10^{-17}/year and $\lesssim 10^{-6}$ with solar potential modulation [18, 21, 22]; mapping these onto κ depends on how ϵ variations propagate to *atomic* lines (captured here by $K_\epsilon^{(S)}$). The clean way to constrain κ is therefore the sector-resolved LPI slope itself, which *directly* measures $K_\epsilon^{(S)}\kappa$.

X. TIKZ CONCEPT SKETCHES

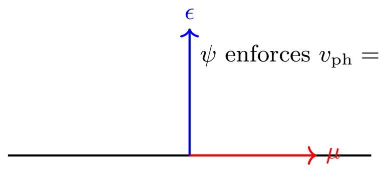

FIG. 1. Dual-sector ψ fabric: ϵ and μ shift oppositely while preserving $v_{\rm ph} = c/n$, consistent with the optical metric.

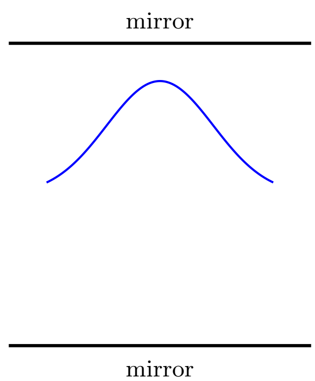

FIG. 2. Fabry–Pérot cavity with TEM_{00} Gaussian profile. Time-averaged *integrated* electric and magnetic energies cancel; paraxial longitudinal fields produce a *local* bracket at $\mathcal{O}(\theta^2)$.

XI. CONCLUSIONS

DFD replaces curved spacetime with a scalar ψ refractive field. It recovers GR's classical tests, resolves Penrose's "two geometries" problem by ensuring a unique ψ with unitary quantum evolution, and predicts a nonzero LPI slope. In the dual-sector extension, Maxwell electrodynamics is consistently embedded in a ψ-dependent vacuum with an ϵ/μ split that preserves $v_{\rm ph} = c/n$. The unified bracket $[B^2/\mu - \epsilon E^2]$ controls energy, momentum, and sourcing, with concrete predictions. Falsifiers: $\xi = 0$ across all cavity–atom pairs (contrary to DFD), no ψ-pumping under designed drive, no sectoral asymmetries under TE/TM swaps, and *any* verified DP-like intrinsic collapse at predicted $\tau_{\rm DP}$ scales.

[1] M. Faraday, "Experimental Researches in Electricity," *Philos. Trans. R. Soc. Lond.* **122**, 125–162 (1831).
[2] J. C. Maxwell, "A Dynamical Theory of the Electromagnetic Field," *Philos. Trans. R. Soc. Lond.* **155**, 459–512 (1865).
[3] O. Heaviside, *Electromagnetic Theory*, articles in *The Electrician* (1888–1891).
[4] J. D. Jackson, *Classical Electrodynamics*, 3rd ed. (Wiley, 1999).
[5] D. J. Griffiths, *Introduction to Electrodynamics*, 5th ed. (Cambridge, 2017).
[6] C. M. Will, *Theory and Experiment in Gravitational Physics*, updated ed. (Cambridge, 2018).
[7] C. J. Bordé, "Theoretical tools for atom optics and interferometry," *C. R. Acad. Sci. Paris* **2**, 509–530 (2001).

[8] P. Storey and C. Cohen-Tannoudji, “The Feynman path integral approach to atomic interferometry. A tutorial,” *J. Phys. II France* **4**, 1999–2027 (1994).
[9] R. Penrose, *The Emperor’s New Mind* (Oxford Univ. Press, 1989).
[10] R. Penrose, *Shadows of the Mind* (Oxford Univ. Press, 1994).
[11] R. Penrose, “On gravity’s role in quantum state reduction,” *Gen. Relativ. Gravit.* **28**, 581–600 (1996).
[12] L. Diósi, “Models for universal reduction of macroscopic quantum fluctuations,” *Phys. Rev. A* **40**, 1165 (1989).
[13] S. Adler and A. Bassi, “Collapse models: Analysis of the free particle dynamics,” *J. Phys. A* **40**, 15083 (2007); A. Bassi et al., *Rev. Mod. Phys.* **85**, 471 (2013).
[14] M. Arndt *et al.*, “Wave–particle duality of C_{60} molecules,” *Nature* **401**, 680–682 (1999).
[15] S. Gerlich *et al.*, “Quantum interference of large organic molecules,” *Nat. Commun.* **2**, 263 (2011).
[16] Y. Y. Fein *et al.*, “Quantum superposition of molecules beyond 25 kDa,” *Nat. Phys.* **15**, 1242–1245 (2019).
[17] A. Vinante *et al.*, “Improved noninterferometric test of collapse models using ultracold cantilevers,” *Phys. Rev. Lett.* **119**, 110401 (2017).
[18] T. Rosenband *et al.*, “Frequency ratio of Al^+ and Hg^+ single-ion optical clocks; stability and systematic uncertainty,” *Science* **319**, 1808–1812 (2008).
[19] P. Delva *et al.*, “Test of special relativity using a fiber network of optical clocks,” *Phys. Rev. Lett.* **121**, 231301 (2018).
[20] N. Ashby *et al.*, “Testing local position invariance with four Cesium-fountain primary frequency standards and four NIST hydrogen masers,” *Phys. Rev. A* **98**, 052507 (2018).
[21] R. M. Godun *et al.*, “Frequency ratio of two optical clock transitions in Yb^+ and constraints on the time variation of fundamental constants,” *Phys. Rev. Lett.* **113**, 210801 (2014).
[22] N. Huntemann *et al.*, “Improved limit on a temporal variation of m_p/m_e from comparisons of Yb^+ and Cs atomic clocks,” *Phys. Rev. Lett.* **113**, 210802 (2014).
[23] C. Eisele, A. Yu. Nevsky, S. Schiller, “Laboratory test of the isotropy of light propagation at the 10^{-17} level,” *Phys. Rev. Lett.* **103**, 090401 (2009).
[24] M. Nagel *et al.*, “Direct terrestrial test of Lorentz symmetry in electrodynamics to 10^{-18},” *Nat. Commun.* **6**, 8174 (2015).
[25] P. Touboul *et al.*, “MICROSCOPE Mission: First Results,” *Phys. Rev. Lett.* **119**, 231101 (2017).
[26] P. Touboul *et al.*, “MICROSCOPE Mission: Final Results,” *Phys. Rev. Lett.* **129**, 121102 (2022).
[27] T. Kessler *et al.*, “A sub-40-mHz-linewidth laser based on a silicon single-crystal optical cavity,” *Nat. Photonics* **6**, 687–692 (2012).
[28] T. Nicholson *et al.*, “Systematic evaluation of an atomic clock at 2×10^{-18} total uncertainty,” *Nat. Commun.* **6**, 6896 (2015).
[29] W. McGrew *et al.*, “Atomic clock performance enabling geodesy below the centimetre level,” *Nature* **564**, 87–90 (2018).